Hydrothermal self-assembly of sodium manganese iron phosphate particles: Growth mechanism and...

Article *in* Solid State Ionics · December 2017

DOI: 10.1016/j.ssi.2017.10.020

6 authors, including:

Claude Karegeya
University of Liège
3 PUBLICATIONS **3** CITATIONS
SEE PROFILE

Abdelfattah Mahmoud
University of Liège
34 PUBLICATIONS **159** CITATIONS
SEE PROFILE

R. Cloots
University of Liège
199 PUBLICATIONS **2,344** CITATIONS
SEE PROFILE

Solid State Ionics 312 (2017) 88–96

Contents lists available at ScienceDirect

Solid State Ionics

journal homepage: www.elsevier.com/locate/ssi

Hydrothermal self-assembly of sodium manganese iron phosphate particles: Growth mechanism and electrochemical performance in lithium-ion battery

Claude Karegeya[a,b], Abdelfattah Mahmoud[a,*], Bénédicte Vertruyen[a], Frédéric Hatert[c], Rudi Cloots[a], Frédéric Boschini[a]

[a] GREENMAT, CESAM, Institute of Chemistry B6, University of Liège, 4000 Liège, Belgium
[b] Faculty of Sciences, College of Education, University of Rwanda, 5039 Kigali, Rwanda
[c] Laboratory of mineralogy B18, University of Liège, 4000 Liège, Belgium

ARTICLE INFO

Keywords:
$Na_2Mn_{1.5}Fe_{1.5}(PO_4)_3$
Alluaudite structure type
Hydrothermal synthesis
Crystal growth mechanism
Mössbauer spectroscopy
Lithium-ion battery

ABSTRACT

$Na_2Mn_{1.5}Fe_{1.5}(PO_4)_3$ (NMFP) dandelion sphere-like particles were successfully synthesized via a hydrothermal route without addition of any templates or surfactants (laboratory and pilot scales). The hydrothermal reactor (pilot scale) is equipped with stirrer for continuous agitation of reagents during the reaction. The obtained materials were characterized by X-ray diffraction, Mössbauer spectroscopy and Scanning electron microscopy. Results show that $Na_2Mn_{1.5}Fe_{1.5}(PO_4)_3$ samples obtained from the reaction performed at laboratory scale have hierarchical dandelion sphere-like morphology and the dandelions consist of micro-/nano-rods. On the other hand, we obtained the self-assembly nano-rods morphology for the particles prepared using hydrothermal reactor. On the basis of the experimental results, a growth mechanism of $Na_2Mn_{1.5}Fe_{1.5}(PO_4)_3$ self-assembly and dandelion sphere-like particles was proposed. Temperature and time of hydrothermal reaction are found to be crucial parameters in controlling the growth of $Na_2Mn_{1.5}Fe_{1.5}(PO_4)_3$ particles. In addition, investigation of the effect of continuous stirring during the hydrothermal reaction shows that the reaction time can be optimized to obtain $Na_2Mn_{1.5}Fe_{1.5}(PO_4)_3$ with small particles size. The influence of stirring on the NMFP morphology has been clearly evidenced. Indeed, the stirring leads to homogeneous particles. Cycling studies have shown that the synthesized $Na_2Mn_{1.5}Fe_{1.5}(PO_4)_3$ dandelions materials exhibit specific discharge capacities of about 62 and 57 mAh g^{-1} equivalent to about 1.2 and 1.05 lithium ions de-intercalated at C/15 and C/10 current density respectively.

1. Introduction

The synthesis of particles with 3D structures has attracted more attention due to their interesting properties and potential technical applications [1–6]. 3D compound architectures are built from one dimensional (e.g. nanowires, nanotubes and nanorods) or two dimensional (e.g. nanoplates) nano/micro-particles which are spontaneously organized in a particular way [7]. These materials have shown promising properties in various fields, especially in energy storage and conversion as electrode materials and in biomedical applications [8–11]. 3D materials have been mainly obtained by soft chemistry synthesis methods and among others solvothermal and hydrothermal methods have been extensively used [12,13]. Hydrothermal and solvothermal syntheses are more effective and convenient in achieving a variety of hierarchical architectures due to their various advantages such as fast reaction kinetics, short processing times, phase purity, high crystallinity, high yield, homogeneous particle products, composite formation and narrow particle-size distributions [14].

During the last decades, the design and the tailoring of the particles with controlled morphology architectures under mild and at low-cost conditions has been an intensive research field. Nevertheless, this issue still remains a great challenge for chemists and material scientists [1]. Here we discuss the synthesis of alluaudite-type sodium manganese iron phosphate ($Na_2Mn_{1.5}Fe_{1.5}(PO_4)_3$), which was obtained by hydrothermal synthesis route, and crystallized in 3D dandelion morphology structure via self-assembly. Alluaudite materials have recently attracted increasing attention as promising cathode materials for next-generation sodium and lithium-ion batteries (NIBs and LIBs) [13–15]. The importance given to iron phosphate-based alluaudite group is due to their stability at high temperature, the presence of vacancies that allow easy intercalation of Na/Li-ions in their crystal structures as well as their environmental friendliness and low cost [16]. They theoretically exhibit low capacities due to their high molecular weight, but the alluaudite structure vacancies owing to their complementarities and

* Corresponding author.
E-mail address: abdelfattah.mahmoud@ulg.ac.be (A. Mahmoud).

http://dx.doi.org/10.1016/j.ssi.2017.10.020
Received 30 July 2017; Received in revised form 18 October 2017; Accepted 22 October 2017

synergetic effect in the insertion/extraction process enhances their capacities and shows good cycling performances as cathode materials for LIBs and NIBs [17–19].

$Na_2Mn_{1.5}Fe_{1.5}(PO_4)_3$ has not been studied as electrode material elsewhere. In this work, it has been well established that a strong correlation exists between the electrochemical properties and the morphology, size, and structure of the inorganic materials. The dandelion nano-/micro architecture may facilitate the entering of electrolyte, sodium or lithium-ions and could provide much more active specific surface. These can lead to fast transport, reduce diffusion paths of Li ions and good cycling performance. 3D dandelion architecture of $Na_2Mn_{1.5}Fe_{1.5}(PO_4)_3$ phase has attracted our attention thanks to the interesting properties doted to alluaudite materials and 3D architecture. The objective of this work is the investigation and optimization of the synthesis conditions used in hydrothermal synthesis of $Na_2Mn_{1.5}Fe_{1.5}(PO_4)_3$ phase. Relationship between structural, morphological characteristic and electrochemical properties will be presented.

2. Experimental

2.1. Synthesis of Na $_2Mn_{1.5}Fe_{1.5}(PO_4)_3$ with 3D dandelion architecture

2.1.1. Synthesis in Teflon-lined stainless steel autoclave

The hydrothermal typical synthesis of $Na_2Mn_{1.5}Fe_{1.5}(PO_4)_3$ material consists on mixing precursors solutions and suspensions and treating the mixture at moderate temperature. In this process, 4 mmol sodium dihydrogen phosphate ($NaH_2PO_4{\cdot}H_2O \geq 99.0\%$, Aldrich) and 8 mmol sodium nitrate ($NaNO_3$, ≥ 99.0%, Aldrich) solutions were mixed with 2 mmol manganese carbonate ($MnCO_3$, ≥ 99.9%, Aldrich) and 2 mmol iron oxalate ($FeC_2O_4{\cdot}2H_2O$, 99.0%, Aldrich) suspensions in 60 mL of milli-Q water. The mixture was stirred for 0.5 h under argon at room temperature. Then, the mixture was sealed into a 125 mL Teflon-lined stainless steel autoclave and heated in oven at various temperatures (180–220 °C) and during different durations (2–6 h). The final products were collected by gravimetric filtration, washed with water and ethyl alcohol several times for each one respectively, and then dried in electric oven under vacuum at 80 °C for 2 h.

2.1.2. Synthesis in hydrothermal reactor equipped with a stirrer

In similar way as the above synthesis reaction in teflon-lined stainless steel autoclave, the mixture of $Na_2Mn_{1.5}Fe_{1.5}(PO_4)_3$ precursors was transferred in a hydrothermal reactor (Parr 4580, 5.5 L, up to 200 bar, 500 °C), then heated at 220 °C for 6 h. During this synthesis, the reaction undergoes a continuous agitation and sampling has been done every 0.5 h on the stirred hydrothermal reaction. Collected samples were washed and dried in similar conditions as the samples obtained using teflon-lined stainless steel autoclave.

2.2. Characterization

Powder X-ray diffraction (XRD) data was collected on a Panalytical PW-3710 powder diffractometer using FeK_α radiation ($\lambda = 1.9373$ Å), operating from $2\theta = 10$ to 100°. The crystal structure was refined by the Rietveld method, starting from the observed powder diffraction pattern and using the DBWS-9807 software [20].

The morphology and particles size of the prepared samples were observed by scanning electron microscopy (XL 30FEG-ESEM, FEI).

^{57}Fe transmission Mössbauer spectroscopy data were recorded by using a constant-acceleration spectrometer with a ^{57}Co (Rh) source at room temperature. The spectrometer was calibrated at room temperature with the magnetically split sextet spectrum of a high-purity α-Fe foil as the reference absorber. The measurements were carried out in the velocity ranges of ± 4 mm s^{-1} with optimal energy resolution. The Mössbauer spectra were fitted with three Lorentzian doublets using Fullham program. In this way, spectral parameters such as quadrupole splitting (Δ), isomer shift (δ), linewidth (r) and relative resonance areas of the different spectral components were determined for the pure sample obtained in laboratory scale way (in Teflon cup without stirring). The validity of fits was judged on the basis of minimizing the number of parameters and χ values.

Electrochemical measurements were performed using coin cells assembled in an argon-filled glovebox. For preparing working electrodes, a mixture of $Na_{1.5}Mn_{1.5}Fe_{1.5}(PO_4)_3$ dandelion structure, carbon black and polyvinylidene fluoride (PVDF) at a weight ratio of 60:20:20 was pasted on a stainless steel grid. The separator was a 25 mm monolayer polypropylene membrane (Celgard). Lithium foil was used as counter and reference electrodes. The electrolyte consisted of a solution of 1 M $LiPF_6$ in ethylene carbonate (EC)/dimethyl carbonate (DMC) (1:1, v/v). Galvanostatic cycling tests of the assembled cells were carried out on Neware Electrochemical Test System (China) in the voltage range of 4.5–2.0 V (vs. Li^+/Li).

3. Results and discussions

3.1. Preparation of $Na_2Mn_{1.5}Fe_{1.5}(PO_4)_3$ material

To study and design the hydrothermal synthesis mechanism of 3D $Na_2Mn_{1.5}Fe_{1.5}(PO_4)_3$ dandelion particle formation, reactions with various synthesis conditions were performed. The preparation of $Na_2Mn_{1.5}Fe_{1.5}(PO_4)_3$ crystallized in 3D dandelion morphology was achieved with an interesting architecture that can be applied as electrode material for LIBs and NIBs. The experimental flowchart process of hydrothermal synthesis evolution of this phase in teflon-lined stainless steel autoclave (laboratory scale) and hydrothermal reactor (pilot scale) is illustrated in Fig. 1. The $Na_2Mn_{1.5}Fe_{1.5}(PO_4)_3$ particles prepared through a laboratory scale synthesis will be so called later LS-NMFP while the particles obtained by a pilot scale synthesis will be denoted PS-NMFP.

3.2. Structure characterizations

The X-ray diffraction patterns of the two samples (LS-NMFP and PS-NMFP) do not show any difference. Fig. 2 displays the powder X-ray diffraction pattern of $Na_2Mn_{1.5}Fe_{1.5}(PO_4)_3$ sample prepared by laboratory scale hydrothermal synthesis route at 220 °C for 6 h. All Bragg peaks can be attributed to the pure and well crystallized $Na_2Mn_{1.5}Fe_{1.5}(PO_4)_3$ alluaudite [PDF 04-012-077]. Experimental

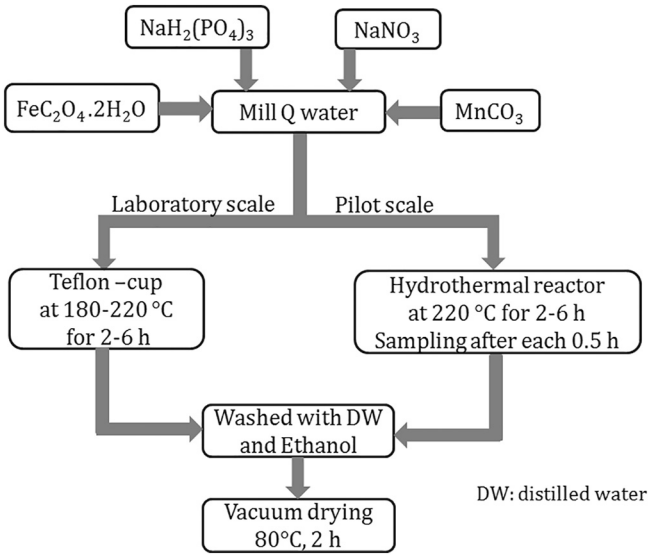

Fig. 1. The process flowchart for synthesis of $Na_2Mn_{1.5}Fe_{1.5}(PO_4)_3$ particles self-assembled in dandelion-like morphologies prepared via hydrothermal synthesis route in stainless steel autoclave and hydrothermal reactor.

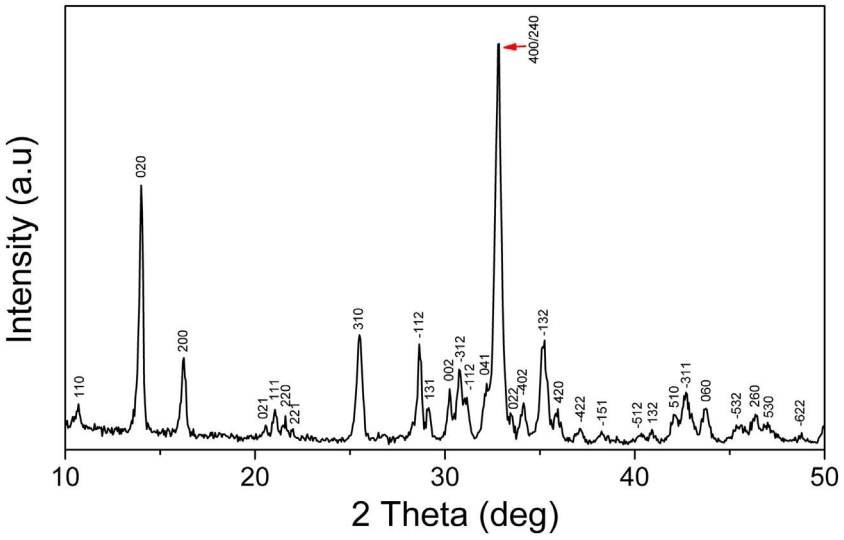

Fig. 2. XRD pattern of $Na_2Mn_{1.5}Fe_{1.5}(PO_4)_3$ sample prepared by laboratory scale hydrothermal synthesis route.

details of the $Na_2Mn_{1.5}Fe_{1.5}(PO_4)_3$ refinement: atomic coordinates, sites occupancies, interatomic distances and angles O-P-O were reported in our recent publication [21] and they are in good agreement with the reported crystal parameters of sodium-manganese-iron-phosphate alluaudite-type phosphate compounds [22–24]. The lattice parameters of dandelion NMFP crystal cell were found to be a = 11.992(1) Å, b = 12.624(1) Å and c = 6.513(1) Å. By comparison with that of standard $Na_2Mn_{1.5}Fe_{1.5}(PO_4)_3$ [PDF 04-012-077]: a = 11.995 Å, b = 12.596 Å and c = 6.495 Å, the lattice parameters show that the crystalline growth of NMFP dandelion particles are in good agreement with experimental crystal data.

3.3. Mössbauer spectroscopy

^{57}Fe Mössbauer spectroscopy was used to study the valence state, local environment and the relative amounts of iron in the $Na_2Mn_{1.5}Fe_{1.5}(PO_4)_3$ samples. The Fig. 3 shows the room temperature ^{57}Fe Mössbauer spectra of the pure $Na_2Mn_{1.5}Fe_{1.5}(PO_4)_3$ samples obtained at 220 °C via laboratory scale (Fig. 3a) and pilot scale (Fig. 3b) syntheses. The corresponding hyperfine parameters are presented in Table 1. The spectra are consistent with the presence of paramagnetic iron, confirming the absence of any magnetic ordering at room temperature. Good quality fits of the data have been obtained using only three doublets.

The isomer shift and quadrupole splitting values for both samples are in good agreement with the existence of one iron site occupied by high-spin Fe(III) and two iron sites occupied by high spin Fe(II) [21]. Indeed, three pronouncedly separated surroundings of Fe ions can be distinguished, which is in good agreement with the XRD results indicating a random distribution of Fe^{2+}, Fe^{3+}, and Mn^{2+} at the M2 site while the M1 site is filled with Mn^{2+} [21].

In both samples (LS-NMFP-6 h and PS-NMFP-0.5 h), the alluaudite structure of $Na_2Mn_{1.5}Fe_{1.5}(PO_4)_3$ compound is preserved. The two compounds exhibit approximately the same isomer shift and quadrupole splitting parameters confirming that the stirring does not significantly modify the s-electron density and the local environment of iron ions in the $Na_2Mn_{1.5}Fe_{1.5}(PO_4)_3$ alluaudite structure. However the Fe^{3+}-content of alluaudites increases in the PS-NMFP-0.5 h sample obtained through the pilot scale route. The oxidation mechanism, which explains these chemical variations, is $Na^+ + Fe^{2+} = [] + Fe^{3+}$. This mechanism is well known as the classical oxidation mechanism affecting natural and synthetic alluaudites [21,25]. Since the oxidation conditions were identical in both experiments, the increase of Fe^{3+} in PS-NMFP-0.5 h could be attributed to the better ordering of cations on their respective sites, favored by a continuous stirring and the higher

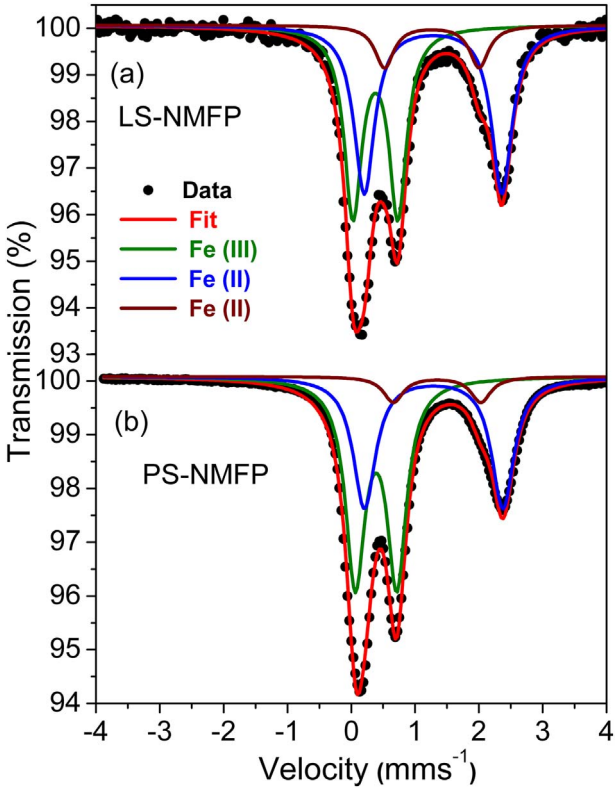

Fig. 3. Room temperature Mössbauer spectra of $Na_2Mn_{1.5}Fe_{1.5}(PO_4)_3$ powder synthesized by hydrothermal method at 220 °C via laboratory scale (6 h) and pilot scale (0.5 h) syntheses.

Table 1
Hyperfine parameters[a] of the room temperature Mossbauer spectra of LS-NMFP (6H) and PS-NMFP (0.5H) samples.

		δ (mm s^{-1})	Δ (mm s^{-1})	Γ (mm s^{-1})	Area (%)
LS-NMFP-6H	Fe(III)	0.37 (4)	0.70 (1)	0.33 (1)	44 (1)
	Fe(II)	1.28 (1)	2.15 (2)	0.38 (1)	46 (1)
	Fe(II)	1.26 (2)	1.48 (5)	0.35 (1)	10 (1)
PS-NMFP-0.5H	Fe(III)	0.39 (1)	0.65 (1)	0.36 (1)	53 (2)
	Fe(II)	1.29 (1)	2.17 (2)	0.42 (1)	40 (1)
	Fe(II)	1.35 (5)	1.37 (1)	0.37 (1)	7 (1)

[a] δ-Isomer shift, referred to α-iron at 295 K, Δ-quadrupole splitting, Γ-line width.

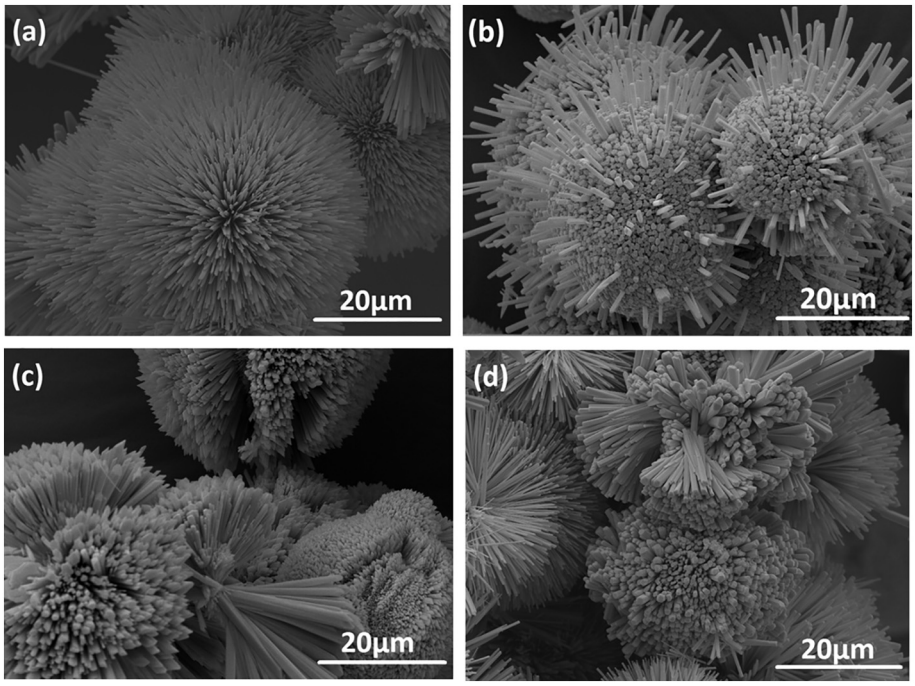

Fig. 4. SEM micrographs of $Na_2Mn_{1.5}Fe_{1.5}(PO_4)_3$ particles prepared by hydrothermal synthesis at 220 °C for 6 h in a teflon-lined stainless steel autoclave.

volume (5.5 L) of the autoclave.

3.4. 3D-$Na_2Mn_{1.5}Fe_{1.5}(PO_4)_3$ dandelion morphology and growth mechanism

Fig. 4 shows the general morphology of the as-prepared 3D $Na_2Mn_{1.5}Fe_{1.5}(PO_4)_3$ phase sample obtained at 220 °C for 6 h in a teflon-lined stainless steel autoclave. Interestingly, the $Na_2Mn_{1.5}Fe_{1.5}(PO_4)_3$ particles can self-organize into spherical assemblies of "dandelions". The 3D dandelions microspheres are in fact built from small crystal strips of one-dimensional (1D) smaller nanofibers. These crystal strips in dandelion sphere-like structure are aligned radially to the spherical surface, pointing toward a common center. In this sample we observed that during 1D nanoparticles growth to form dandelion sphere-like particles, some nanofibers grow with the same speed to form sphere like particles (Fig. 4a) or with different speeds and extra growth of nanofibers were observed (Fig. 4b) or a combination of the two mechanisms (Fig. 4c and d).

To investigate the growth mechanism of the $Na_2Mn_{1.5}Fe_{1.5}(PO_4)_3$ dandelion sphere-like particles, the influence of the annealing time and temperature on the phase purity and particles morphology was investigated throughout this study. On one hand by fixing the temperature of the reaction at 220 °C and varying the time of reaction (2,3,4 and 6 h), on another hand the reaction temperature was varied from 180 °C to 220 °C by maintaining the reaction time at 6 h. In addition the effect of stirring during the hydrothermal reaction was also studied.

3.4.1. Reaction time effect

The formation process of dandelion sphere-like structure, samples obtained at 220 °C at different reaction times of 2, 4 and 6 h have been investigated by XRD and SEM techniques (Fig. 5). X-ray powder diffraction was used to check the phase purity and to confirm the crystal structure of the pure material. The evolution of XRD patterns and particles morphology with hydrothermal reaction time is shown in the Fig. 5. After 2 h of reaction (Fig. 5a and a'), the XRD pattern shows a mixture of several compounds, the sample is composed predominantly by $FePO_4{\cdot}H_2O$ (PDF 04-017-2782) and $Na_7Fe_4(PO_2)_6$ (PDF 04-011-1178), as intermediate reaction compounds with the formation of small quantity of $Na_2Mn_{1.5}Fe_{1.5}(PO_4)_3$ material. The corresponding particles morphology shows rough surface sphere-like particles. This corresponds to the nucleation step in which precursors self-organize to form the particles growth sites. By extending the reaction time to 4 h, X-ray diffraction shows the main peaks of $Na_2Mn_{1.5}Fe_{1.5}(PO_4)_3$ and few peaks with low intensity (Fig. 5b) that correspond to $FePO_4{\cdot}H_2O$. The SEM analysis of this sample phase shows microsphere core formation, and dandelion-like particles start growing from sphere center (Fig. 5b′). When the reaction time was extended to 6 h, the 3D-dandelions architecture was formed (Fig. 5c′), and the corresponding XRD patterns (Fig. 5c) shows that pure phase of $Na_2Mn_{1.5}Fe_{1.5}(PO_4)_3$ was obtained exempt of any impurity. The narrowness of the X-ray diffraction lines indicates a crystallinity of this material even when it is prepared at relatively low temperature.

3.4.2. Reaction temperature effect

After optimization of the synthesis time, and concluding that the pure NMFP material was obtained at 220 °C during 6 h, we undertook a second research focused on the effect of another key parameter which is the effect of hydrothermal temperature on the compositional, structural, morphological and electrochemical properties of NMFP sample. NFMP material was prepared at different hydrothermal reaction temperatures of 180 °C, 200 °C and 220 °C during 6 h.

The comparison of the XRD patterns and micrographs clearly evidenced that the composition and the morphology of the particles are strongly affected by the hydrothermal reaction temperature. XRD pattern of sample obtained at 180 °C for 6 h (Fig. 6a) shows that there are few peaks corresponding to $Na_2Mn_{1.5}Fe_{1.5}(PO_4)_3$ phase and the mixture is mostly composed of intermediate compounds of $FePO_4{\cdot}H_2O$ (PDF 04-017-2782) and $Na_7Fe_4(PO_2)_6$ (PDF 04-011-1178). The corresponding particles morphology (Fig. 6a′) shows agglomeration of particles. This corresponds to the nucleation step, the characteristic SEM micrographs are almost equal to the particle morphology for the sample synthesized at 220 °C for 2 h. When the reaction temperature was increased to 200 °C (Fig. 6b and b′), the corresponding XRD pattern of this sample (Fig. 6b) shows that the main peaks correspond to $Na_2Mn_{1.5}Fe_{1.5}(PO_4)_3$. Indeed, at 200 °C, the intensity of the peaks assigned to the impurities have significantly decreased indicating that at this temperature the impurity percentage is substantially lower and only very small quantity of $FePO_4{\cdot}H_2O$ is detected. The particles were grown enough to form 3D-

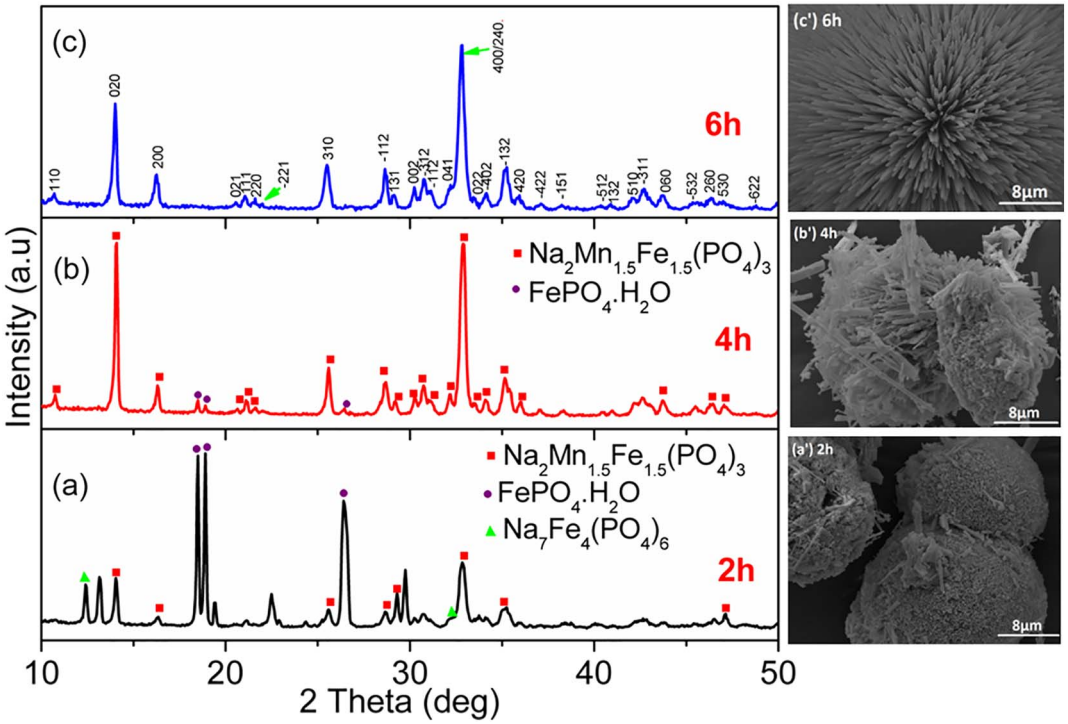

Fig. 5. $Na_2Mn_{1.5}Fe_{1.5}(PO_4)_3$ time-dependent dandelions microspheres formation. XRD patterns (a, b and c) and corresponding morphologies (a′, b′ and c′) of $Na_2Mn_{1.5}Fe_{1.5}(PO_4)_3$ powder synthesized by hydrothermal method at 220 °C after 2, 4 and 6 h reaction time respectively.

dandelion sphere-like particles with various diameter sizes. This shows that some reactants have not reacted at this temperature to form pure $Na_2Mn_{1.5}Fe_{1.5}(PO_4)_3$ phase. This confirms that the phases obtained at 200 °C (Fig. 6b) and below (Fig. 6a) show the presence of impurity phases, even when other conditions were unaltered. The $Na_2Mn_{1.5}Fe_{1.5}(PO_4)_3$ phase exempt of any impurity was obtained when the reaction temperature was fixed at 220 °C for 6 h (Fig. 6c) with particles self-assembled in 3D-dandelion morphology (Fig. 6c′). This result confirms that 220 °C is high enough to obtain high purity NMFP-sample.

3.4.3. *Effect of stirring on the $Na_2Mn_{1.5}Fe_{1.5}(PO_4)_3$ morphology*

In addition to the reaction temperature and time, we investigated also the influence of stirring during hydrothermal reaction on the morphological properties of NMFP-material. In this study, we found that continuous stirring is another added influencing parameter among

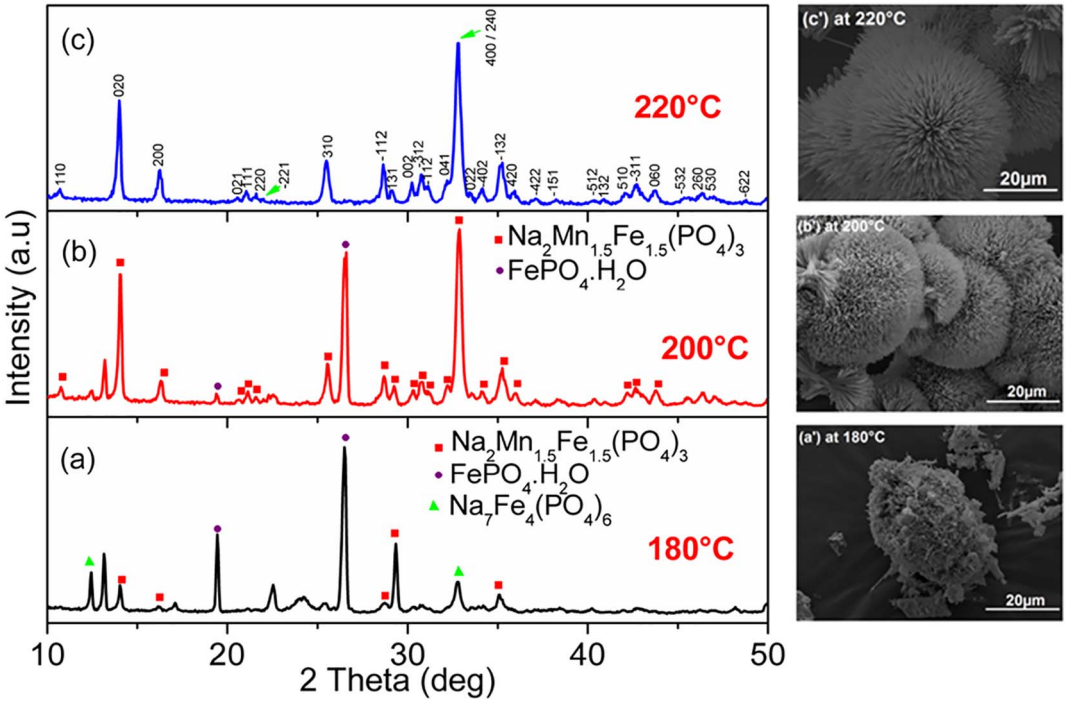

Fig. 6. XRD patterns (a, b and c) and corresponding SEM images (a′, b′ and c′s) of $Na_2Mn_{1.5}Fe_{1.5}(PO_4)_3$ powder synthesized by hydrothermal method after 6 h of reaction time at 180 °C (a'), 200 °C (b′) and 220 °C (c′) respectively.

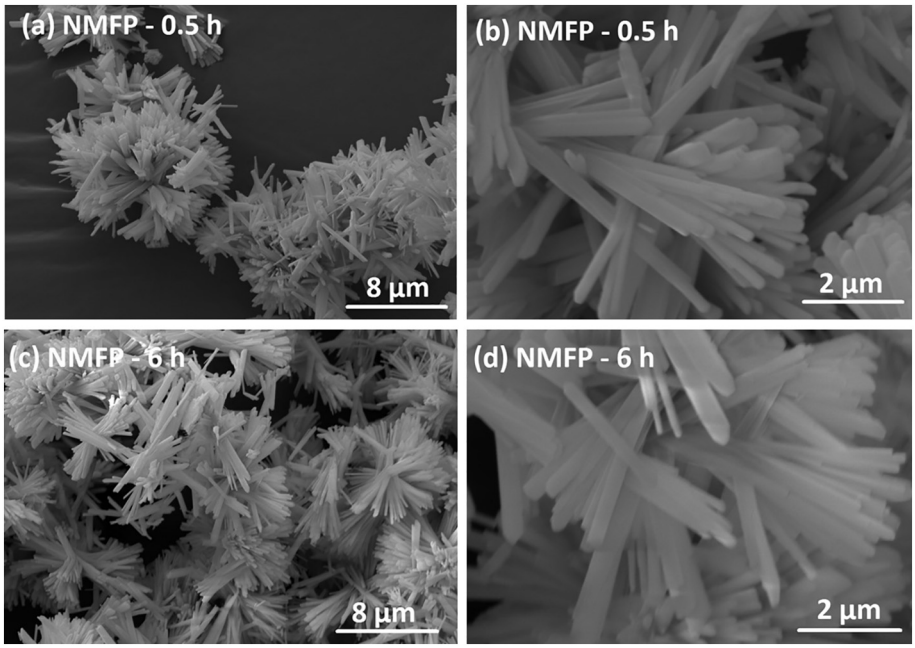

Fig. 7. SEM micrographs of PS-NMFP samples obtained at 220 °C for (a, b) 0.5 h and (c, b) 6 h in a hydrothermal reactor (with stirring).

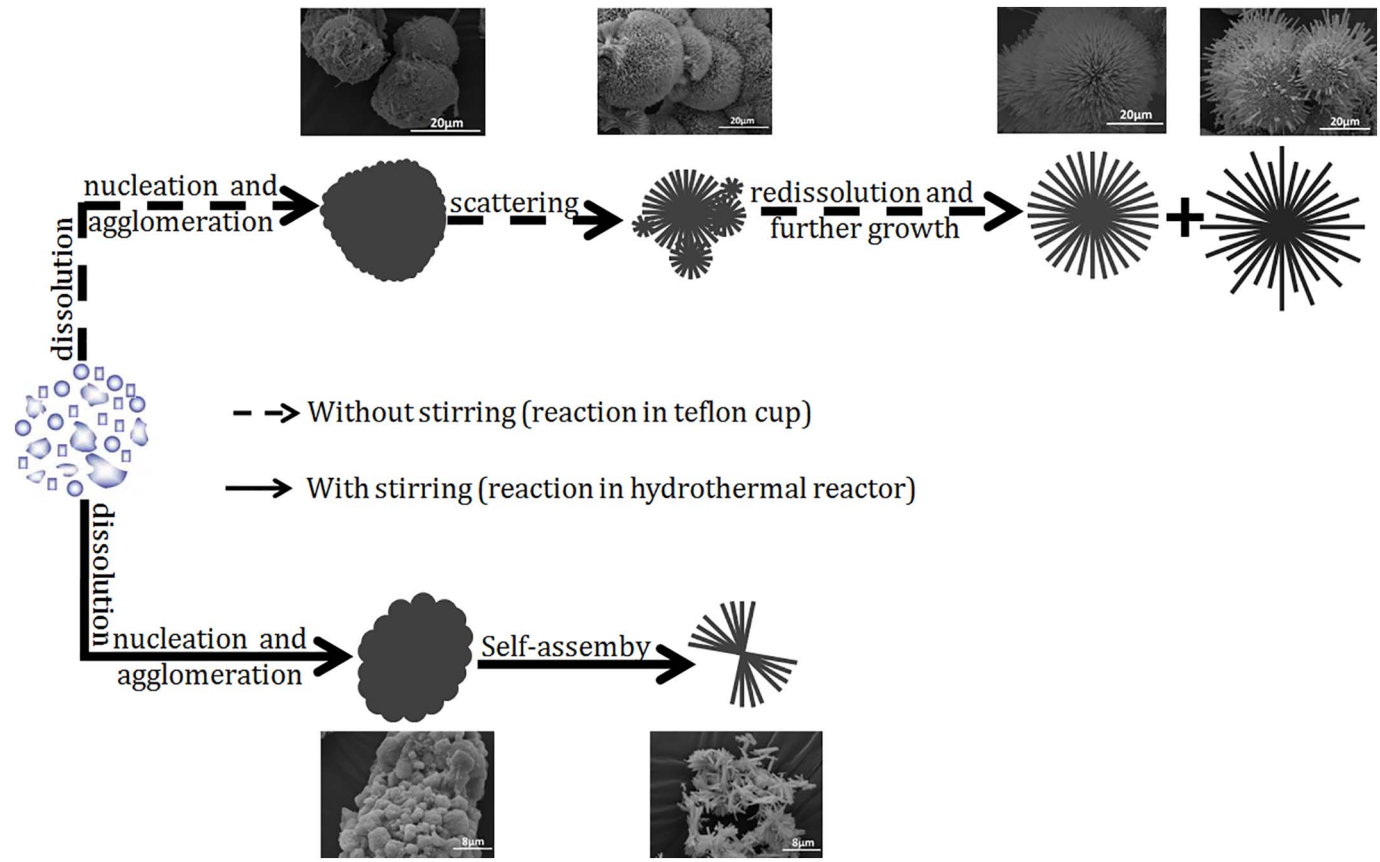

Fig. 8. Schematic representation of $Na_2Mn_{1.5}Fe_{1.5}(PO_4)_3$ morphological growth process during laboratory scale and pilot scale hydrothermal syntheses.

others such as reaction time, reaction temperature and type of additive on the morphology of the prepared materials. In this study, we found that the reaction time and particles morphology are strongly dependent on continuous stirring effect during hydrothermal reaction. The reaction time was reduced from 6 h to 0.5 h (Fig. 7a and b) and the particles morphology is more homogeneous compared to the hydrothermal reaction in a teflon cup (Fig. 4). This shows that the continuous stirring leads to the formation of many homogeneous nuclei and increases particles contact which results in rapid reaction. The uniform dandelions-like particle morphology were the exclusive products (Fig. 7). It was very interesting to observe that the pure $Na_2Mn_{1.5}Fe_{1.5}(PO_4)_3$ phase was obtained with self-assembled particles in dandelion only after 0.5 h of reaction (Fig. 7a and b). The increase of reaction duration from 0.5 h to 6 h (Fig. 7c and d) in pilot scale synthesis did not show

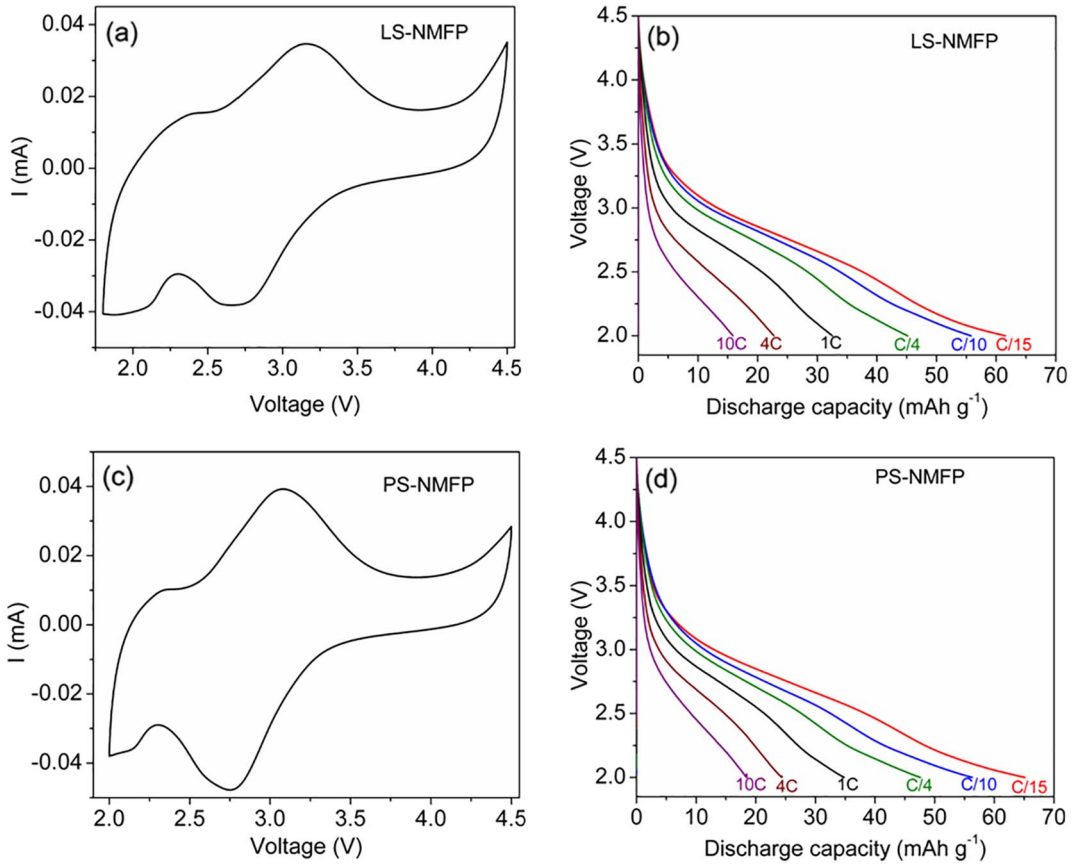

Fig. 9. Schematic of a typical cyclic voltammograms at 0.5 mV s^{-1} scan speeds for $Na_2Mn_{1.5}Fe_{1.5}(PO_4)_3$ obtained through, (a) laboratory scale (LS-NMFP)and (c) pilot scale (PS-NMFP) syntheses. Specific discharge capacity vs. voltage at various current rates of (a) LS-NMFP and (b) PS-NMFP samples in 2.0–4.5 V.

any clear effect on size and morphology of $Na_2Mn_{1.5}Fe_{1.5}(PO_4)_3$ particles. On the contrary, the hydrothermal reaction without continuous stirring in teflon cup, uniform and non-uniform dandelions were observed and some of them show extra particles growth from sphere-like particles (Fig. 4b and d). Therefore the formation of $Na_2Mn_{1.5}Fe_{1.5}(PO_4)_3$ dandelions sphere-like particles depends on the temperature and time of reaction but also the continuous stirring of the reaction mixture.

According to the experimental results above, we proposed a possible growth mechanism of $Na_2Mn_{1.5}Fe_{1.5}(PO_4)_3$ sample with dandelion morphology in Fig. 8. Concerning two reactions carried out in the absence of stirring (teflon-lined stainless steel autoclave) and in hydrothermal reactor equipped with the stirrer respectively. Obviously the two systems experienced similar reaction processes. However the stirring effect leads to the reduction of steps.

In the teflon-lined stainless steel autoclave process, the morphological evolution process involves a change from 0D aggregates of tiny particles to 3D dandelion architectures by means of self-assembly. In the first step, the initially formed suspension particles are aggregated, with a spherical morphology, indicating a nucleation-aggregation mechanism. By approaching the reaction ideal synthesis conditions, the concentration of reactants decreases, the reaction rate slows down, the crystal growth rate gradually becomes dominant, and the prickly $Na_2Mn_{1.5}Fe_{1.5}(PO_4)_3$ crystals appear in dandelion sphere-like aggregates at the end of synthesis process. By controlling the temperature and the time of reaction, samples have a tendency to gradually form the single pure phase from the mixed intermediate phases (Figs. 5 and 6). Meanwhile, it can be seen that the morphology of particles of the initial, intermediate, and final stages of samples preparation are progressively enhanced to the benefits of dandelion sphere-like particles formation. The obtained results indicate that our hydrothermal synthesis protocol provides an appropriate crystal growth environment for the formation of such an interesting 3D architecture.

However, using hydrothermal reactor equipped with the stirrer, the morphology transformation process was similar to the reaction process observed in the absence of continuous stirring (teflon-lined stainless steel autoclave) but the number of steps and reaction time is extensively reduced. In this process, only two steps were identified: nucleation and agglomeration of nanoparticles and finally to the 3D–dandelions appearance. The possible formation mechanisms of 3D $Na_2Mn_{1.5}Fe_{1.5}(PO_4)_3$ hierarchical architectures with dandelion shapes under studied experimental conditions are schematically proposed in Fig. 8.

3.5. Electrochemical properties of $Na_2Mn_{1.5}Fe_{1.5}(PO_4)_3$

Fig. 9 shows the electrochemical properties of LS-NMFP and PS-NMFP cathode materials obtained through laboratory scale (LS-NMFP) and pilot scale (PS-NMFP) syntheses, respectively (procedure shown Fig. 1). For both samples LS-NMFP and PS-NMFP the cyclic voltammograms of $Na_2Mn_{1.5}Fe_{1.5}(PO_4)_3$ cathode material was carried at scan rate of 0.5 mV s^{-1} in 2.0–4.5 V voltage range vs. Li^+/Li. A peak in the cathodic response is observed at about 2.7 V, which could be attributed to the reduction of Fe^{3+} and Mn^{3+} and in the reverse voltage scan the anodic peak at 3.3 V corresponds to the reversible oxidation of Fe^{2+} and Mn^{2+} (Fig. 9a and c).

Fig. 9b and d show the discharge voltage profiles of LS-NMFP and PS-NMFP samples respectively in 2.0–4.5 V voltage range under various current densities (C/15, C/10, C/10, 1C, 4C and 10C). The increase of discharge rate does not noticeably alter the representative discharge curve of NMFP electrode material. However the discharge curves decreases with increasing of the current density which leads to the

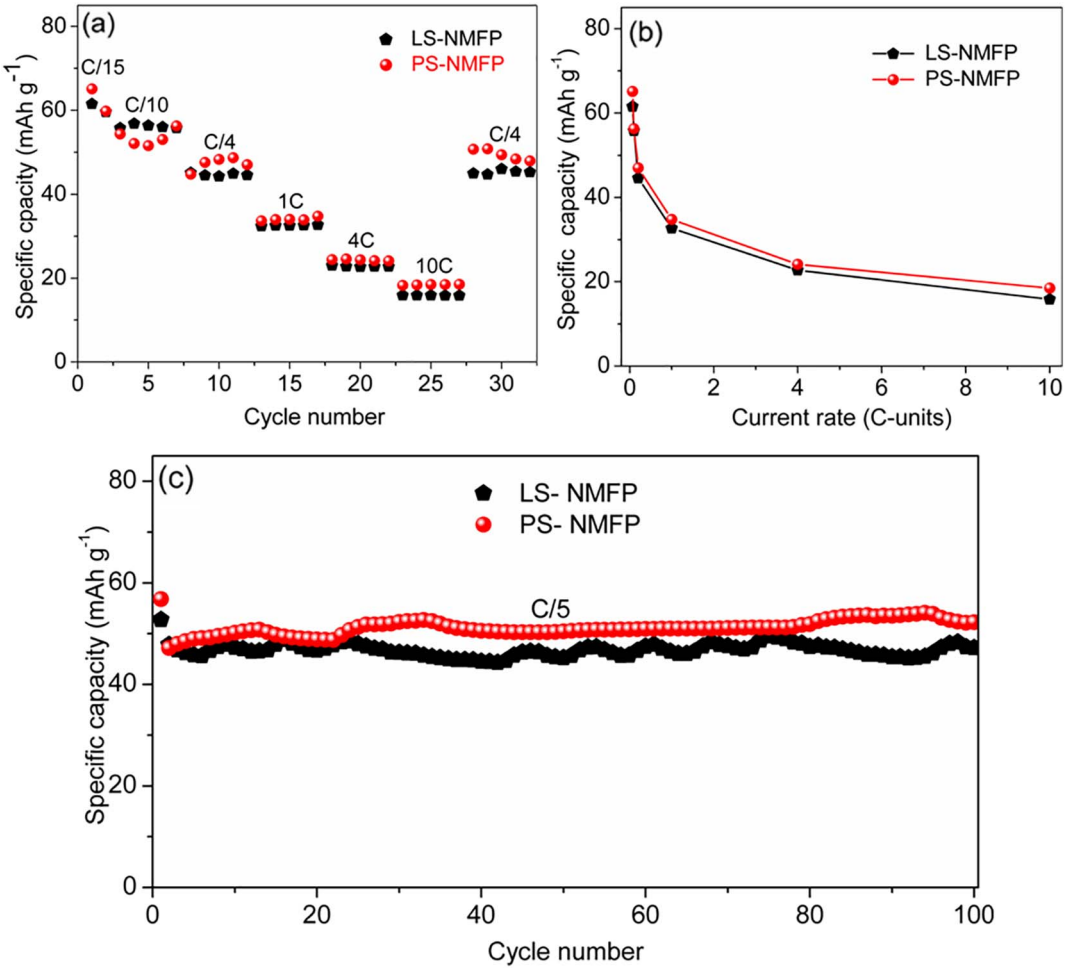

Fig. 10. (a) Rate capability at various current rates, (b) Evolution of discharge capacity as a function of discharge rate and (c) cycling stability at C/5 in 2.0–4.5 V voltage range.

increases of the polarization of the electrode material which decreases the discharge capacity [26].

Indeed, as expected, the discharge capacity decreases for both electrodes with an increase of the discharge current density due to the limited lithium diffusion at high rates. In both samples (LS-NMFP and PS-NMFP) the discharge curves shape illustrate a good Na/Li-extraction/insertion in the $Na_2Mn_{1.5}Fe_{1.5}(PO_4)_3$ cathode material at different current densities. However, It is observed that for all rates, the capacity of the PS-NMFP sample is the highest, suggesting that this sample has the best rate capability and cycling behavior.

In the cyclic voltammetry, the redox peaks can give information about the relative rates of reactions in the electrochemical system [27]. The electrochemical properties of the two samples (LS-NMFP and PS-NMFP) cannot be clearly distinguished in the voltammogram cycles and discharging voltage curves because of their equal operation voltages. However the height of redox peaks for PS-NMFP sample is slightly higher than in LS-NMFP. This justifies the better intercalation/deintercalation of Li-ion in PS-NMFP and leads to slightly better capacities compared to LS-NMFP samples.

The rate performances are shown in Fig. 10a, the electrode presents stable cycling behavior at various applied current densities of C/15, C/10, C/4, 1C, 4C, 10C and C/4. Although the reversible capacity decreases slightly with the increase of discharge rate, the obtained discharge capacities are relatively good at all regimes. At C/15, C/10, C/4, 1C, 4C and 10C current densities, LS-NMFP dandelion sphere-like particles delivers discharge capacities of about 62, 56, 44, 33, 23 and 16 mAh g^{-1} respectively. The Peukert plot (Fig. 10b) shows that the two samples show similar curves evolution. However the discharge capacity values of LS-NMFP are smaller than those of the PS-NMFP sample. This is due to the effect of particles size on electrochemical performances of the NMFP-based cathode materials [28] as we found that PS-NMFP particles are smaller than LS-NMFP particles (Figs. 4 and 7). As we restored to cycling rate to C/4 after 27 cycles, the PS-NMFP sample delivers the discharge capacity of 44 mAh g^{-1} with excellent recovery of 100%. This result demonstrated that the alluaudite structure of the NMFP material is not destroyed during the rate capability studies.

$Na_2Mn_{1.5}Fe_{1.5}(PO_4)_3$ should exhibit a maximum theoretical capacity (3 eq. $*$ 53.8 = 161 mAh g^{-1}) if it cycled between the end members $Mn^{III}_{1.5}Fe^{III}_{1.5}(PO_4)_3$ and $Na_2(Na,Li)Mn^{II}_{1.5}Fe^{II}_{1.5}(PO_4)_3$ by exchanging three Li^+/Na^+ equivalents [17]. However the previous studies on the Na-Mn-Fe-Phosphate-based alluaudites have shown that this class of materials can only transfer 2 e^- [18,29]. Hence, the $Na_2Mn_{1.5}Fe_{1.5}(PO_4)_3$ corresponding theoretical capacity is 108 mAh g^{-1}.

Even though the theoretical capacity of $Na_2Mn_{1.5}Fe_{1.5}(PO_4)_3$ ($\sim$108 mAh g^{-1}) is low, this material shows the high cycling reversibility (Fig. 10c) with a capacity retention of $>$ 99% at 100th cycle for both samples PS-NMFP and LS-NMFP. This shows that the 3D-$Na_2Mn_{1.5}Fe_{1.5}(PO_4)_3$ material is identified as a promising electrode material thanks to its alluaudite structure properties and 3D- dandelion architecture.

4. Conclusions

The 3D-dandelion $Na_2Mn_{1.5}Fe_{1.5}(PO_4)_3$ architectures morphologies

have been successfully synthesized by a hydrothermal method in laboratory scale and pilot scale processes, respectively. The morphology and the dimensions of the product change remarkably with the reaction conditions such as reaction time, temperature and stirring effect. The possible formation mechanisms for 3D $Na_2Mn_{1.5}Fe_{1.5}(PO_4)_3$ architecture are proposed based on time, temperature and stirring-dependent experiments.

The nucleation and growth conditions are well controlled in our synthesis protocol based on temperature and time-dependent experiments. The continuous stirring during hydrothermal reaction was identified as another crucial hydrothermal reaction parameter which influences the reaction and particles morphology. This parameter may be extended to the fabrication of other inorganic materials in order to get uniform particles morphology and reduce hydrothermal reaction time. The 3D-dandelion architecture leads to particles with small size which leads to large surface area. The analysis and measurements of electrochemical properties of 3D $Na_2Mn_{1.5}Fe_{1.5}(PO_4)_3$ material shows good reversible electrochemical properties. This justifies the good performance of $Na_2Mn_{1.5}Fe_{1.5}(PO_4)_3$ dandelion morphology which deliver 62 mAh g^{-1} and 57 mAh g^{-1} capacity equivalent to about 1.2 and 1.05 lithium ions intercalated at C/15 and C/10 respectively. In addition the material stability, structural vacancies, availability and low cost of precursors used during synthesis make $Na_2Mn_{1.5}Fe_{1.5}(PO_4)_3$ a promising electrode material. 3D-dandelion sphere-like morphology enhances its electrochemical performance as cathode material for Li-ion batteries. This confirms that the morphology is an important parameter that affects electrochemical properties. We recommend that the synthesis protocol used here may be used in production of other interesting electrode materials in 3D-architecture in order to improve their electrochemical properties.

Acknowledgements

The authors are grateful to University of Liege and FRS-FNRS for equipment grants. Part of this work was supported by the Walloon Region under the “PE PlanMarshall2.vert” program (BATWAL – 1318146). C. Karegeya acknowledges the abroad study leave of the University of Rwanda. A. Mahmoud is grateful to the Walloon region for a Beware Fellowship Academia 2015-1, RESIBAT no 1510399.

References

[1] L. Xu, J. Shen, C. Lu, Y. Chen, W. Hou, Self-assembled three-dimensional architectures of $Y_2(WO_4)_3$:Eu: controlled synthesis, growth mechanism, and shape-dependent luminescence properties, Cryst. Growth Des. 9 (2009) 3129–3136.
[2] B.B. Kale, J.-O. Baeg, S.M. Lee, H. Chang, S.-J. Moon, C.W. Lee, $CdIn_2S_4$ nanotubes and “Marigold” nanostructures: a visible-light photocatalyst, Adv. Funct. Mater. 16 (2006) 1349–1354.
[3] N. Eshraghi, S. Caes, A. Mahmoud, R. Cloots, B. Vertruyen, F. Boschini, Sodium vanadium (III) fluorophosphate/carbon nanotubes composite (NVPF/CNT) prepared by spray-drying: good electrochemical performance thanks to well-dispersed CNT network within NVPF particles, Electrochim. Acta 228 (2017) 319–324.
[4] K. Lasri, A. Mahmoud, I. Saadoune, M.-T. Sougrati, L. Stievan, P.-E. Lippens, R.P. Hermann, H. Ehrenberg, Toward understanding the lithiation/delithiation process in $Fe_{0.5}TiOPO_4$/C electrode material for lithium-ion batteries, Sol. Energy Mater. Sol. Cells 148 (2016) 11–19.
[5] X. Wu, G. Shi, S. Wang, P. Wu, Formation of 3D dandelions and 2D nanowalls of copper phosphate dihydrate on a copper surface and their conversion into a nanoporous CuO film, Eur. J. Inorg. Chem. 2005 (2005) 4775–4779.
[6] C. Karegeya, A. Mahmoud, R. Cloots, B. Vertruyen, F. Boschini, Hydrothermal synthesis in presence of carbon black: pa rticle-size reduction of iron hydroxyl phosphate hydrate for Li-ion battery, Electrochim. Acta 250 (2017) 49–58.
[7] A. Lak, M. Mazloumi, M. Mohajerani, A. Kajbafvala, S. Zanganeh, H. Arami, S.K. Sadrnezhaad, Self-assembly of dandelion-like hydroxyapatite nanostructures via hydrothermal method, J. Am. Ceram. Soc. 91 (2008) 3292–3297.
[8] L.-S. Zhong, J.-S. Hu, H.-P. Liang, A.-M. Cao, W.-G. Song, L.-J. Wan, Self-assembled 3D flowerlike iron oxide nanostructures and their application in water treatment, Adv. Mater. 18 (2006) 2426–2431.
[9] P. Yu, X. Zhang, Y. Chen, Y. Ma, Self-template route to MnO_2 hollow structures for supercapacitors, Mater. Lett. 64 (2010) 1480–1482.
[10] X. He, M. Yang, P. Ni, Y. Li, Z.-H. Liu, Rapid synthesis of hollow structured MnO_2 microspheres and their capacitance, Colloids Surf. A Physicochem. Eng. Asp. 363 (2010) 64–70.
[11] M. Sadat-Shojai, M.-T. Khorasani, E. Dinpanah-Khoshdargi, A. Jamshidi, Synthesis methods for nanosized hydroxyapatite with diverse structures, Acta Biomater. 9 (2013) 7591–7621.
[12] H. Wen, M. Cao, G. Sun, W. Xu, D. Wang, X. Zhang, C. Hu, Hierarchical three-dimensional cobalt phosphate microarchitectures: large-scale solvothermal synthesis, characterization, and magnetic and microwave absorption properties, J. Phys. Chem. C 112 (2008) 15948–15955.
[13] X. Zhang, P. Yu, Y. Chen, Y. Ma, Low-temperature hydrothermal synthesis of α-MnO_2 three-dimensional nanostructures, Mater. Lett. 64 (2010) 583–585.
[14] M.K. Devaraju, I. Honma, Hydrothermal and solvothermal process towards development of $LiMPO_4$ (M = Fe, Mn) nanomaterials for lithium-ion batteries, Adv. Energy Mater. 2 (2012) 284–297.
[15] C. Nan, J. Lu, C. Chen, Q. Peng, Y. Li, Solvothermal synthesis of lithium iron phosphate nanoplates, J. Mater. Chem. 21 (2011) 9994–9996.
[16] P.P. Prosini, Iron Phosphate Materials as Cathodes for Lithium Batteries: the Use of Environmentally Friendly Iron in Lithium Batteries, Springer Science & Business Media, 2011.
[17] K. Trad, D. Carlier, L. Croguennec, A. Wattiaux, M. Ben Amara, C. Delmas, $NaMnFe_2(PO_4)_3$ alluaudite phase: synthesis, structure, and electrochemical properties as positive electrode in lithium and sodium batteries, Chem. Mater. 22 (2010) 5554–5562.
[18] R. Essehli, H.B. Yahia, K. Maher, M.T. Sougrati, A. Abouimrane, J.-B. Park, Y.-K. Sun, M.A. Al-Maadeed, I. Belharouak, Unveiling the sodium intercalation properties in $Na_{1.86}Mn_{014}Fe_3(PO_4)_3$, J. Power Sources 324 (2016) 657–664.
[19] W. Huang, B. Li, M.F. Saleem, X. Wu, J. Li, J. Lin, D. Xia, W. Chu, Z. Wu, Self-assembled Alluaudite $Na_2Fe_{3-x}Mn_x(PO_4)_3$ micro/nanocompounds for sodium-ion battery electrodes: a new insight into their electronic and geometric structure, Chem. Eur. J. 21 (2015) 851–860.
[20] R.A. Young, A.C. Larson, C.O. Paiva-Santos, Rietveld analysis of X-ray and neutron powder diffraction patterns, Sch. Phys. Ga. Inst. Technol, Atlanta GA, http://debian.ccp14.ac.uk/ccp/web-mirrors/dbws/downloads/young/guide99.pdf, (1998) , Accessed date: 3 February 2017.
[21] C. Karegeya, A. Mahmoud, B. Vertruyen, F. Hatert, R.P. Hermann, R. Cloots, F. Boschini, One-step hydrothermal synthesis and electrochemical performance of sodium-manganese-iron phosphate as cathode material for Li-ion batteries, J. Solid State Chem. 253 (2017) 389–397.
[22] F. Hatert, L. Rebbouh, R.P. Hermann, A.-M. Fransolet, G.J. Long, F. Grandjean, Crystal chemistry of the hydrothermally synthesized $Na_2(Mn_{1-x}Fe_x^{2+})_2Fe^{3+}(PO_4)_3$ alluaudite-type solid solution, Am. Mineral. 90 (2005) 653–662.
[23] F. Hatert, Crystal chemistry of the divalent cation in alluaudite-type phosphates: a structural and infrared spectral study of the $Na_{1.5}Mn_{1.5}Fe_{1.5}(PO_4)_3$ solid solutions (x = 0 to 1, M^{2+} = Cd^{2+}, Zn^{2+}), J. Solid State Chem. 181 (2008) 1258–1272.
[24] F. Hatert, G.J. Long, D. Hautot, A.-M. Fransolet, J. Delwiche, M.-J. Hubin-Franskin, F. Grandjean, A structural, magnetic, and Mössbauer spectral study of several Na–Mn–Fe-bearing alluaudites, Phys. Chem. Miner. 31 (2004) 487–506.
[25] F. Hatert, Etude cristallochimique et synthèse hydrothermale des alluaudites: contribution nouvelle au problème génétique des phosphates de fer et de manganèse dans les pegmatites granitiques et, partant, à celui de l'évolution de ces gisements, http://orbi.ulg.ac.be/handle/2268/102892, (2004) , Accessed date: 16 June 2017.
[26] A. Mahmoud, J.M. Amarilla, K. Lasri, I. Saadoune, Influence of the synthesis method on the electrochemical properties of the $Li_4Ti_5O_{12}$ spinel in Li-half and Li-ion full-cells. A systematic comparison, Electrochim. Acta 93 (2013) 163–172.
[27] J. Wu, X.Z. Yuan, H. Wang, M. Blanco, J.J. Martin, J. Zhang, Diagnostic tools in PEM fuel cell research: part I electrochemical techniques, Int. J. Hydrog. Energy 33 (2008) 1735–1746.
[28] A. Mahmoud, J.M. Amarilla, I. Saadoune, Effect of thermal treatment used in the sol–gel synthesis of $Li_4Ti_5O_{12}$ spinel on its electrochemical properties as anode for lithium ion batteries, Electrochim. Acta 163 (2015) 213–222.
[29] V. Palomares, P. Serras, I. Villaluenga, K.B. Hueso, J. Carretero-González, T. Rojo, Na-ion batteries, recent advances and present challenges to become low cost energy storage systems, energy, Environ. Sci. 5 (2012) 5884–5901.